International Journal of Modern Manufacturing Technologies
ISSN 2067–3604, Vol. XVII, No. 1 / 2025
https://doi.org/ 10.54684/ijmmt.2025.17.1.170

SYNTHESIS OF NICO-BIMETALLIC NITRIDE/GRAPHENE OXIDE/TI_3C_2 MXENE HYBRID ELECTRODE FOR SUPERCAPACITORS

Elendu Ekwueme Samson[1], Eris Elianddy Supeni[2], Mohd Khairol Anuar Mohd Arffin[3], Suhadi Shafie[4], Muhammad Ishaq[5]

[1-4]Department of Mechanical & Manufacturing Engineering, Facuty of Engineering, Universiti Putra Malaysia, 43400 UPM Serdang Selangor Darul Ehsan, Malaysia
[5]School of Chemistry and Chemical Engineering, Shanghai Electrochemical Energy Device Research Center Shanghai Jiao Tong University Shanghai, China

Corresponding author: Eris Elianddy Supeni, eris@upm.edu.my

Abstract: It is becoming more widely acknowledged that energy storage technologies are essential to achieving sustainable development objectives. Effective energy storage technologies are essential for improving grid stability, permitting greater integration of renewable energy, and lowering dependency on fossil fuels as international efforts to slow down climate change and switch to renewable energy sources increase. By addressing intermittency issues and facilitating the efficient utilization of renewable resources such as solar and wind power, advancements in energy storage contribute significantly to building resilient, low-carbon energy systems essential for sustainable development. The goal of this work is to improve the specific capacitance, rate capability, and cycling stability of supercapacitors by synthesizing and characterizing a novel hybrid electrode material made of reduced graphene oxide, bimetallic NiCo-nitride, and Ti_3C_2 MXene. The two-step synthesis technique created a bimetallic NiCo-nitride/reduced graphene oxide/Ti_3C_2 MXene hybrid from NiCo-layered double hydroxide (LTHs) on a flexible nickel foam substrate (named NCN@rGO/Ti_3C_2/NF). First, NC-LDH@rGO/Ti_3C_2/NF nanosheets were grown hydrothermally in situ on the nickel foam surface. This was followed by thermal annealing in an NH_3 environment at temperatures between 300 and 500°C. Based on electrochemical measurements, the NCN@rGO/Ti_3C_2/NF hybrid electrode annealed at 500°C (NCN@rGO/Ti_3C_2/NF-500) showed exceptional cycling stability of 93.8% after 3500 cycles and excellent rate capability of 92.2% at 20 Ag-1. Its specific capacitance reached 1032.71 Fg-1 at 0.5 Ag-1.

Key words: NiCo-nitride, reduced graphene oxide, Ti_3C_2 MXene hybrid, nickel foam, super capacitor

1. INTRODUCTION

Renewable energy storage technologies are replacing nuclear energy and fossil fuels like coal, oil, and natural gas in the energy sector [1]. Overuse of fossil fuels has raised significant concerns about energy and environmental problems in society. In order to solve these issues, green and renewable energy sources such as nuclear, solar, wind, and tidal energy which have emerged as competitive alternatives energy [2]. Maybe nuclear energy is starting to show promise as a fossil fuel substitute. However, the advancement of nuclear technology has been significantly slowed down by a number of catastrophic incidents [3]. However, the development of effective energy storage technology is essential to use the intermittent nature of solar, wind, and tidal power sources. More effective and efficient energy storage solutions must be developed in light of the growing popularity of portable devices and the rise in power consumption [4]. They were the most widely available energy storage devices at the time because of their great energy density, such as portable gadgets and electric cars (EVs). Modern Li-ion batteries still have safety concerns, a low power density, and a short cycling life, nevertheless [5]. As opposed to Li-ion batteries, which rely on redox processes in the bulk materials for charge storage, supercapacitors (SCs), also known as electrochemical capacitors or ultracapacitors, store energy through rapid and reversible ion adsorption/desorption at the electrode/electrolyte interface. [6]. Because of its high-power density, quick charging and discharging times, robust cyclic stability, and superior safety, SCs have attracted a lot of attention [7]. However, energy densities of SCs are relatively low (about 5–10 Wh kg−1), significantly limit their potential for widespread use, encouraging the development of innovative smart material syntheses and designs, such as metallic nitrides and hierarchical metallic oxide/hydroxide nanocomposites. Due to their exceptional electrical conductivity and enhanced sustainability, these nanocomposites have demonstrated efficacy in expanding energy-based technologies and are widely acknowledged as a successful

method of achieving great energy density without compromising cycle life or power density. The remarkable electrochemical characteristics of SCs, including their rapid charging and discharging rate, excellent specific power, and extended cycling life, have drawn a wide spectrum of research interest. [8]. As an adaptable energy storage system, SCs have garnered international attention since their introduction to the market. Conventional the charge storage capacity of capacitors ranges from micro to millifarads (F), whereas SCs have a range of 100 to 1000 F for each device while maintaining low equivalent series resistance (ESR) and specific power. SCs could cover both the specific energy density (Ed) and power density (Pd) by several orders of magnitude compared to batteries by utilizing proper design and efficient materials. The Energy Information Administration (EIA) of the United States (U.S.) predicted that the global supercapacitor market is estimated to be USD 6.29 billion in 2022 and is projected to reach USD 17.93 billion by 2027, increasing by almost at a CAGR of 23.3%, as illustrated in Figure 1a [10]. More effective sustainable energy production and storage may result from electrochemical energy conversion and storage technology [11]. On the other hand, electrochemical energy systems, such as fuel cells, batteries, supercapacitors, and capacitors, can be installed in any climate and consistently generate electricity wherever. Various electrochemical energy storage devices' efficiency [12, 13]. Their particular properties, such as energy/power densities, cyclability, and efficiency, make them valuable for commercial purposes [14]. These systems share many additional characteristics, which can also be explained by the crucial difference in their energy storage technique (physical *vs.* electrochemical). Although electrical charge transfer across the material's bulk may give electrochemical batteries and fuel cells higher energy densities (100-200 Wh kg-1/600-1200 Wh kg-1), these devices are more prone to degradation and have lower cyclability than electrochemical capacitors [15].

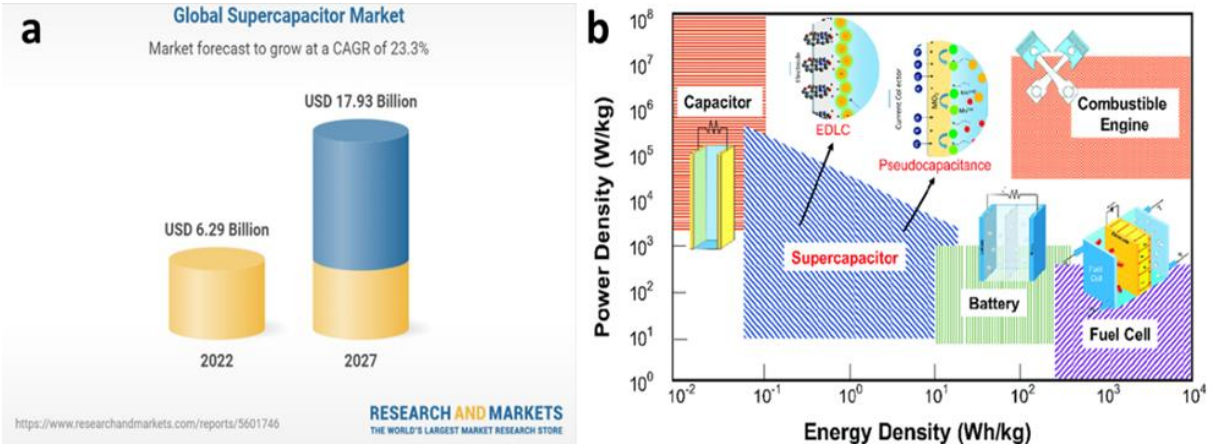

Fig. 1. (a) Global supercapacitor market projection. Data source: The world largest research and market. [https://www.researchandmarkets.com/reports/5601746/global- supercapacitor-market- 2022-2027]. (b) Ragone diagram depicting the efficiency of various electrochemical energy storage systems [9]

2. RESEARCH METHODOLOGY

2.1. Materials and chemicals

All of the chemical reagents, unless specified otherwise, were bought from Aladdin Chemical Co. Ltd. and were of excellent grade (95.0 to 99.5%). Ultra-purified water (UP), having a resistivity of 18.2 MΩ•cm, was used during the experiment.

2.2. Nickel foam pre cleaning

The nickel foam, designated NF, was cut to dimensions of 20 mm by 40 mm by 1 mm. Then, using an ultrasonic bath with an amplitude of 80% for 15 minutes and a solution made of 10% HCl, acetone, and ultrapure water, the surface oxide layer was carefully removed. To enable the solvent to drain, the NF was subsequently dried in a vacuum oven at 60°C for 12 hours.

2.3. Graphene oxide synthesis

The Hummers process has been carried out to create graphene oxide (GO) [16]. Generally, 2.5 g of sodium nitrate ($NaNO_3$) and 5 g of natural graphite powder (45 µm lateral size, 99% purity) were combined with 115 milliliters of sulfuric acid (H_2SO_4, 98.08%) in concentrated form. The liquid was then spun for half an hour in an ice bath that was set at 5°C. After that, the suspension was supplemented with 15 g of $KMnO_4$. The flask was placed in a water bath and maintained at 35°C for 30 minutes. For the next 30 minutes of Ultra-purified water (UP), which had a resistance of 18.2 MΩ•cm, was employed in the experiment. A burette was utilized to

gradually add 230 milliliters of water to the solution. The suspension was then heated to 98 degrees Celsius. The resultant suspension was further diluted after 15 minutes to around 420 ml, and 50 ml of 30% peroxide was added. The centrifugation, washing, and drying processes were used to obtain the graphite oxide powder. Using a Front Ultrasonic (FRQ-1006HT, 300W) ultrasonic bath (Germany), the graphite oxide was ultrasonically exfoliated to create the GO.

2.4. Synthesis of mxene

Initially, 1 g of LiF and 15 mL of 8 M HCl were combined to create the etchant. After that, 1 g of Ti_3AlC_2 (MAX) powder was gradually added to the aforesaid solution, and the mixture was kept at 35 °C for a full day. The collected mixture was kept at a pH of 7 until it was centrifuged with deionized water for 10 minutes each cycle at 5000 rpm. Then deionized water was combined with Ti3C2 (MXene), and the mixture was bath sonicated in an ice bath for one hour. The dark green MXene solution (5 mg/mL) was collected after 5 minutes of centrifugation at 3500 rpm for further use.

2.5. Synthesis of NC-N@rGO/Ti_3C_2/NF hybrid

The NC-N@rGO/Ti_3C_2/NF Hybrids Were Fabricated *Via* a Two-Step Method. **Step 1**: Growth of NC-N@rGO/Ti_3C_2/NF in situ, the homogeneous precipitation hydrothermal approach will be used to create nano sheets on the nickel foam's surface. Table 1. displays the optimal molar ratios. Usually, 80 milliliters of ultrapure water with a suspension of GO (80 mg) and MXene (20 mg) was used to dissolve Ni $(NO_3)_2{\cdot}6H_2O$ (0.005 M) and $CoCl_2{\cdot}4H_2O$ (0.0025 M). In order to create a brownish-green solution, the mixture was sonicated for one hour after being agitated for ten minutes at room temperature. Then, the solution was stirred for half an hour with urea (0.025 mole) dissolved in 20 ml of water. The resulting combination and the prepared nickel foam were then put into a 120 ml autoclave vessel lined with Teflon and kept at 180 °C in an electric oven for a further 12 hours. The NC-LDH@rGO/Ti_3C_2 hybrid was rinsed with ultrapure water and ethanol ultrasonic multiple times after the autoclave vessel naturally cooled to room temperature. It was then dried in a vacuum oven for 12 hours at 60 °C. **Step 2**: NC-N@rGO/Ti_3C_2/NF hybrid was derived from NC-LDH@rGO/Ti_3C_2/NF precursor by thermal annealing in NH_3 atmosphere (80-100 ml/min) for 3 h at different temperature (400, 500 and 600 ˚C) at 5 ˚C/min. The obtained electrode was labeled as NCN@rGO/Ti_3C_2/NF-400, NCN@rGO/Ti_3C_2/NF-500, and NCN@rGO/Ti_3C_2/NF-600, respectively.

Table 1. Optimized molar ratios for experimentation

Optimized molar ratios			mg		ml
$Ni(NO_3)_2{\cdot}6H_2O$	$CoCl_2{\cdot}6H_2O$	Urea	GO	Ti_3C_2	H_2O
0.005	0.005	0.025	80	40	80
0.005	0.0025	0.025	80	20	80
0.005	0.0016	0.025	80	10	80

2.6. Electrochemical measurements

All electrochemical measurements of the NCN@rGO/Ti_3C_2/NF electrodes with different ratios were carried out on a electrochemical workstation (CHI660C, China) utilizing a common three-electrode cell deprived of any additive/binder. When conducting electrochemical tests in a 6 M KOH electrolyte at room temperature, all generated materials were used as working electrodes. The captive and reference electrodes were made of platinum foil and a saturated calomel electrode (SCE), respectively. Their intended uses can be carried out with great caution using cyclic voltammetry (CV). The cycle life was directed on a LAND CT2001A test system by galvanostatic charge-discharge technique, and explored the cycling performance of the obtained electrode materials. The voltametric measurements occur within a potential range of 0 to 0.6 V (vs. SCE) at different scan rates of 6, 8, 10, 15, and 20 Hz, respectively. GCD curves were measured at different current densities 6, 8,10,15, 20 A/g in the potential range of 0-0.55 V (vs. SCE). Cycle stability measurements were tested at 20 Ag^{-1} for 2000 cycles. Data from electrochemical impedance measurements (EIS) were gathered at an open circuit potential with an AC voltage amplitude of 5 mV in the frequency range of 100 kHz to 0.01 Hz. The following equation can be used to calculate the specific capacitance.

$$C_s = I\Delta t/m\Delta V \quad (1)$$

where C_s is the specific capacitance (F g^{-1}), I is the discharge current (A), ΔV is the potential drop during discharge (V), m is the mass of the active materials in the electrode (g), and Δt is the discharge time (s).

Energy density E, (Wh kg^{-1}) and power density P (W kg^{-1}) were calculated from the discharge curves according to the following equation:

$$E = Cm(\Delta V)^2/8 \quad (2)$$

$$P = E/\Delta t \quad (3)$$

where Cm, ΔV, and Δt are the mass-specific capacitance, cell voltage (1.5 V), and discharge time, respectively.

3. RESULTS AND DISCUSSION

Creating a bimetallic NiCo-nitride/reduced graphene oxide/Ti_3C_2 MXene hybrid on a flexible nickel foam (NF) substrate (designated as NCN@rGO/Ti_3C_2/NF) as an electrode devoid of binder with improved electrochemical characteristics for uses of super capacitors (SC) was the primary driving force behind this project's effort. A schematic representation of the innovative NCN@rGO/Ti_3C_2/NF synthetic method is shown in **Figure 2.** There are two important phases in it. First, using in situ hydrothermal reactions between Ni(II) salts, Co(II) salts, and urea, the greenish pink precursor of bimetallic NiCo-layered double hydroxide (LDH) nanosheets was grown over the surface of nickel foam substrate. The characteristic amount of Ni (II) salts and Co(II) salts were obtained. dissolved by sonication and stirring in a GO and Mxene solution.

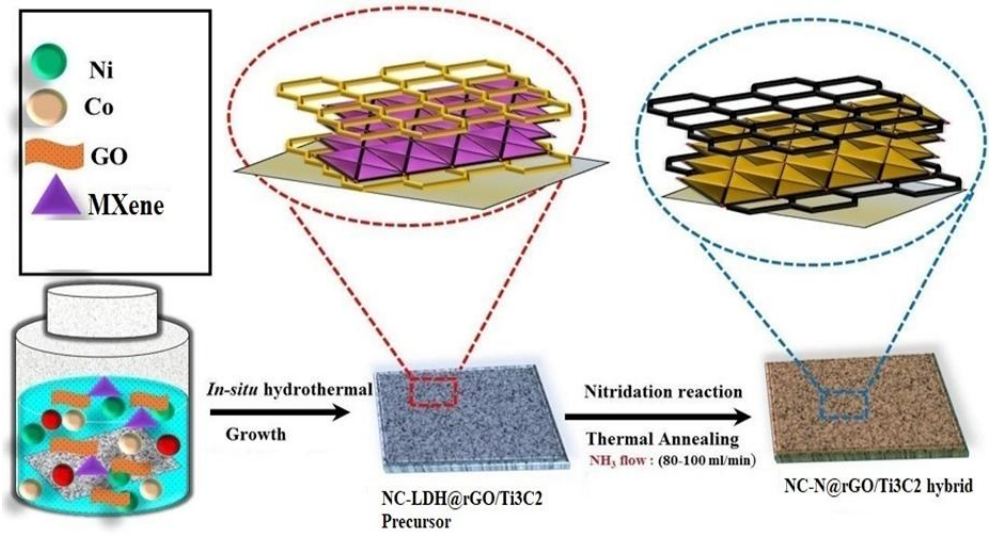

Fig. 2. Schematic representations for the formation mechanism of NC-N@rGO/Ti_3C_2 Hybrid

Under stirring, the solution was combined with a urea solution. Because of the electrostatic force of attraction and hydrogen bonding between the GO and MXene's are essential components of the necessary structural design. In the subsequent step, the obtained NC-LDH@rGO/Ti_3C_2/NF Nano sheets precursor was calcined in NH3 atmosphere (80-100ml/min) for 3 h at different temperatures (400, 500 and 600˚C) at 5˚C/min negative negatively charged function groups ((-O, -OH, and -F) and the NI^{2+}-ION and CO^{2+}-ION, a stable colloidal solution was created.. The precursor hybrid was then obtained by converting the solution into a hydrothermal reaction and treating it for 12 hours at 180 °C in an electric oven. As a cross-linker and dispersion for NiCo-layered double hydroxide (LDH) nanosheets during the hydrothermal process, GO and Mxene The obtained electrode was labeled as NCN@rGO/Ti_3C_2/NF-400, NCN@rGO/Ti_3C_2/NF-500, and NCN@rGO/Ti_3C_2/NF-600, respectively. Figure 3 displays NC-LDH@rGO/Ti_3C_2/-1, NC-LDH@rGO/Ti_3C_2/-2, NC-LDH@rGO/Ti_3C_2/-3 precursor hybrid, and NCN@rGO/Ti_3C_2/-3(300ºC), NCN@rGO/Ti3C2/- 3(400 ºC) and NCN@rGO/Ti_3C_2/-3(500ºC) hybrid at annealing temperatures of 300, 400, and 500ºC. The OH stretching vibration mode of the OH functional group and water molecules in the interlayer was responsible for the broad peak at 3473 cm1 and the shoulder peak at 1639 cm^{-1} in Figure 3a for the NC-LDH@rGO/Ti_3C_2/-1, NC-LDH@rGO/Ti_3C_2/-2, and NC-LDH@rGO/Ti_3C_2/-3 samples. The ü3 bending vibration of the CO^{2-}ion may be responsible for the peaks at 1375 and 771 cm^{-1}. The Stretching and bending vibrations of metal-oxygen (M-O) in crystals was attributed to all other bands below 800 cm^{-1}, indicating that the NiCo-LDH precursor was successfully obtained. All of the spectra of the metal-OH (~3433), C=N (~1631), C=C (~1404), and metal-N (~1039) exhibited the distinctive peaks. NCN@rGO/Ti_3C_2/-3(300 ºC), NCN@rGO/Ti_3C_2/-3(400 ºC), and NCN@rGO/Ti_3C_2/- 3(500 ºC) hybrid after nitration in NH_3 gas flow at 300, 400, and 500 ºC (Figure 3b). This implies that the creation of a surface functional bond composite was accomplished. At temperatures between

300 and 400 ºC, nitride nanoparticles are assembled, meaning that by 500 ºC, to become nitride, the hexagonal structure has undergone a complete transformation. nanoparticles. For the cathode in super capacitors, these different morphological landscapes are thought to provide the following benefits: (1) Without the addition of a polymeric binder, Effective charge transfer is produced by the close electrical contact between the NC-N nanoparticles and the rGO/MXene/NF layers below, and (2) a large number of electrochemically active sites are exposed as a result of the nanoparticles' formation. Similarly, a comprehensive nanostructure investigation of the NC- LDH@GO/Ti_3C_2/-3 precursor and NC- N@GO/Ti_3C_2/-3 hybrid annealed at 500 ºC was conducted using transmission electron microscopy (TEM).

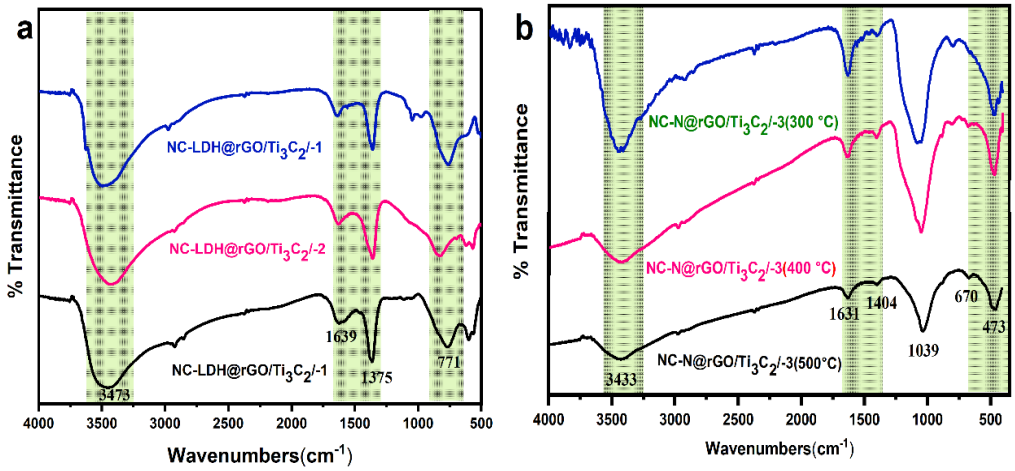

Fig. 3 (a) FT-IR spectra of NC-LDH@rGO/Ti_3C_2/-1, NC-LDH@rGO/Ti_3C_2/-2, and NC-LDH@rGO/Ti_3C_2/-3 precursor hybrid. (b) NC-N@rGO/Ti3C2/-3(300ºC), NCN@rGO/Ti_3C_2(400ºC) and NCN@rGO/Ti_3C_2/-3(500ºC) hybrid at various annealing temperatures, namely 300, 400, and 500 ºC

3.1. Measurement via electrochemistry

An analysis of the electrochemical performance of active materials utilizing a half-wavelength gap is used to compare the ideal metallic ratio of NC-LDH@GO/Ti_3C_2/-1, NC-LDH@GO/Ti_3C_2/-2, and NC-LDH@GO/Ti_3C_2/-3 precursor for the fabrication of NC-N@GO/Ti_3C_2 hybrid electrode. cell three-electrode system in 6 M KOH aqueous electrolyte by cyclic voltammetry (CV), galvanostatic charge- discharge measurement. Figure 4(a-c) shows the cyclic voltammograms (CVs) of the NC- LDH@GO/Ti_3C_2/-1, NC-LDH@GO/Ti_3C_2/-2, and NC- LDH@GO/Ti_3C_2/-3 precursor electrodes, recorded at the scan rate of 5 mv/s with a range of potential between 0 and 0.6 V (versus SCE). During the charge and discharge cycles, Faradaic redox reactions occur at the surface of all LDH nanostructures., as demonstrated by the clear pair of redox peaks that emerged in both the cathodic and anodic portions of all the curves. Considering the earlier research, [17]. The redox reactions of LDH- Ni+2/LDH (OH−) -Ni+3, and LDH-Co+2/LDH (OH−) -Co+3 in alkaline electrolytes proceed according to the following equations:

LDH Ni+2 + OH- sol ↔ LDH (OH-) - Ni+3 + e- (4)
LDH Co+2 + OH- sol ↔ LDH(OH-) - Co+3 + e- (5)

Figure 4(d-f), shows the comparative galvanostatic charge−discharge (GCD) curves of the three NC-LDH@GO/Ti_3C_2/-1, NC-LDH@GO/Ti_3C_2/-2, and NC-LDH@GO/Ti_3C_2/-3 precursor hybrid at different current density. Every curve displayed an equilateral nonlinear form and redox behavior similar to that of a battery; this confirmed that those redox reactions were taking place during the charge-discharge procedures. As anticipated, the NC- LDH@GO/Ti_3C_2/-3 hybrid electrode has the longest discharge time, suggesting the highest capacity for charge storage. For NC- LDH@GO/Ti_3C_2/-3, the specific capacitances were determined to be 1032.2 F/g at a density of current of 1 A/g., 615.8 F/g for NC-LDH@GO/Ti_3C_2/-2, 442.2 F/g for NC- LDH@GO/Ti_3C_2/-1 hybrid (Figure 4g). Moreover, the GCD curves of NC-LDH@GO/Ti_3C_2, with different current densities, and the estimated specific capacitances values as a result of various current densities (1.0-10 A/g), based on the discharge periods of NC-LDH@GO/Ti_3C_2/-3, NC- LDH@GO/Ti_3C_2/-2, and NC-LDH@GO/Ti_3C_2/-1, hybrid are plotted in Figure 4(d-f). One could see that NC- LDH@GO/Ti_3C_2/-3 revealed evidently stable and higher specific Capacitance compared to other hybrid electrodes at any current density. The estimated specific capacitance values were about 1032.7, 996.8, 913.3, 901.6, and 892.1 F/g at 1, 2, 4, 8, and10 A/g with retention rates of 86.4% for NC-LDH@GO/Ti_3C_2/-3, and 615.8, 598.7, 589.3, 559.1, and 544.3 F/g at 1-10 A/g

with retention rates of 88.3 % for NC-LDH@GO/Ti_3C_2/-2. Similarly, 442.2, 385.8, 325.2, 302.1, and 286.3 F/g at 1, 2, 4, 8, and 10 A/g with retention rates of 64.7 % for NC- LDH@GO/Ti_3C_2/-1.

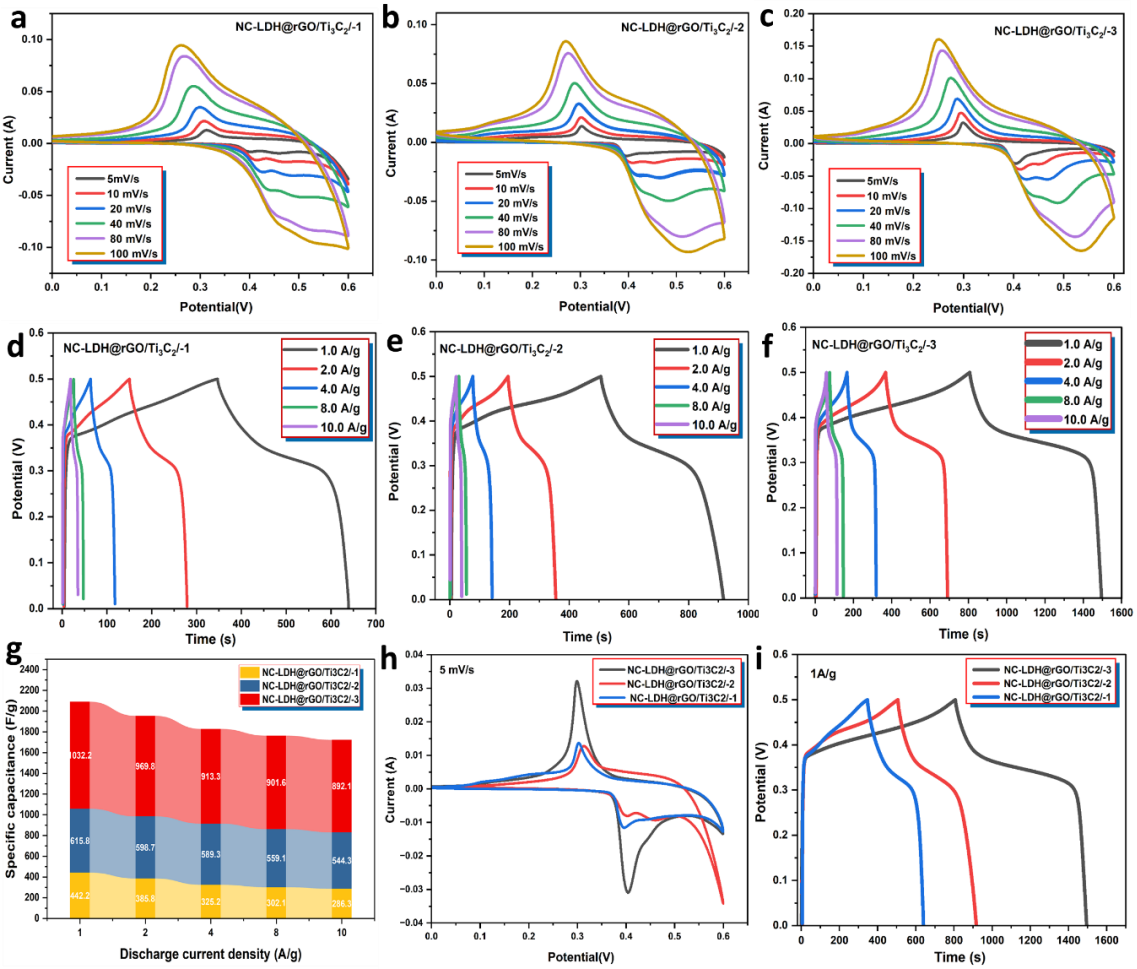

Fig. 4. (a-c) CV curves of NC-LDH@GO/Ti_3C_2/-1, NC-LDH@GO/Ti_3C_2/-2, and NC-LDH@GO/Ti_3C_2/-3 hybrid precursors at a scan rate of 5 mV/s. (d-f) GCD curves and (g) histogram of the specific capacitance of the hybrids at various current densities. (h) CV curves of NC-LDH@GO/Ti_3C_2/-1, NC-LDH@GO/Ti3C2/-2, and NC-LDH@GO/Ti_3C_2/-3 precursor at 5 mV/s and (i) GCD curves of NC-LDH@GO/Ti_3C_2/-1, NC-LDH@GO/Ti_3C_2/-2, and NC-LDH@GO/Ti_3C_2/-3 precursor at 1.0 A/g

Furthermore, the synergistic interaction between conductive GO/Ti_3C_2/-3 and NC-LDH is primarily responsible for the increased specific capacitance of the NC-LDH@GO/Ti_3C_2/-3 hybrid. Moreover, at the same feeding ratio (3:1), NC- LDH@GO/Ti_3C_2/-3 hybrid exhibited higher specific capacitance than NC-LDH@GO/Ti_3C_2/-2 and NC-LDH@GO/Ti_3C_2/-1. These variations in the NC-LDH@GO/Ti_3C_2/-3 hybrid's specific capacitances could be the result of GO/Ti_3C_2's better electrical conductivity, which was measured to be 148 S/m for NC-LDH@GO/Ti_3C_2/-1, 189 S/m for NC-LDH@GO/Ti_3C_2/-2, and 249 S/m for NC- LDH@GO/Ti_3C_2/-3. Figure 4(h and i) show the comparative CV and GCD profile for all three ratio samples.

Specifically, it is significant to see that the relative redox peak CV area and the discharge profile time of NC-LDH@GO/Ti_3C_2/-3 hybrid are larger than those of other electrodes presented (NC- LDH@GO/Ti_3C_2/-3 > NC-LDH@GO/Ti_3C_2/-2 > NC- LDH@GO/Ti_3C_2/-1), suggesting its superior highest average specific capacitance and pseudocapacitive characteristics. Additionally, the CV redox peak positions of the hybrids were slightly different, possibly due to the irreversibility in the faradaic process and worse inherent phase stability of the NiCo-LDH in NC-LDH@GO/Ti_3C_2/-1, NC-LDH@GO/Ti_3C_2/-2, and NC- LDH@GO/Ti_3C_2/-3 hybrid. The NC-LDH@GO/Ti_3C_2/-3 precursor hybrid was selected for the nitridation process based on the overall electrochemical performance. Figure 4(A-C) shows the CV curves of NC- N@GO/Ti_3C_2/-3(300ºC), NC-N@GO/Ti_3C_2/- 3(400ºC) and NC-N@GO/Ti_3C_2/-3(500ºC) hybrid electrodes annealed at temperatures of 300, 400, and 500 degrees Celsius, with a possible window of 0 to 0.6 V (*vs.* SCE). Evidently, the pseudo capacitance behavior of the fabricated metallic nitride active materials is demonstrated by the pair of strong redox peaks seen in each of the separate CV curves. Following cycling at different scan rates (5-100 mV/s), the

primary reduction and oxidation peaks coincide with a little shift toward higher potential, indicating the excellent reversibility of the NC-N@GO/Ti_3C_2/-3(300ºC), NC-N@GO/Ti_3C_2/-3(400ºC), and NC-N@GO/Ti_3C_2/-3(500ºC) electrodes as shown in Figure 4(d-f).

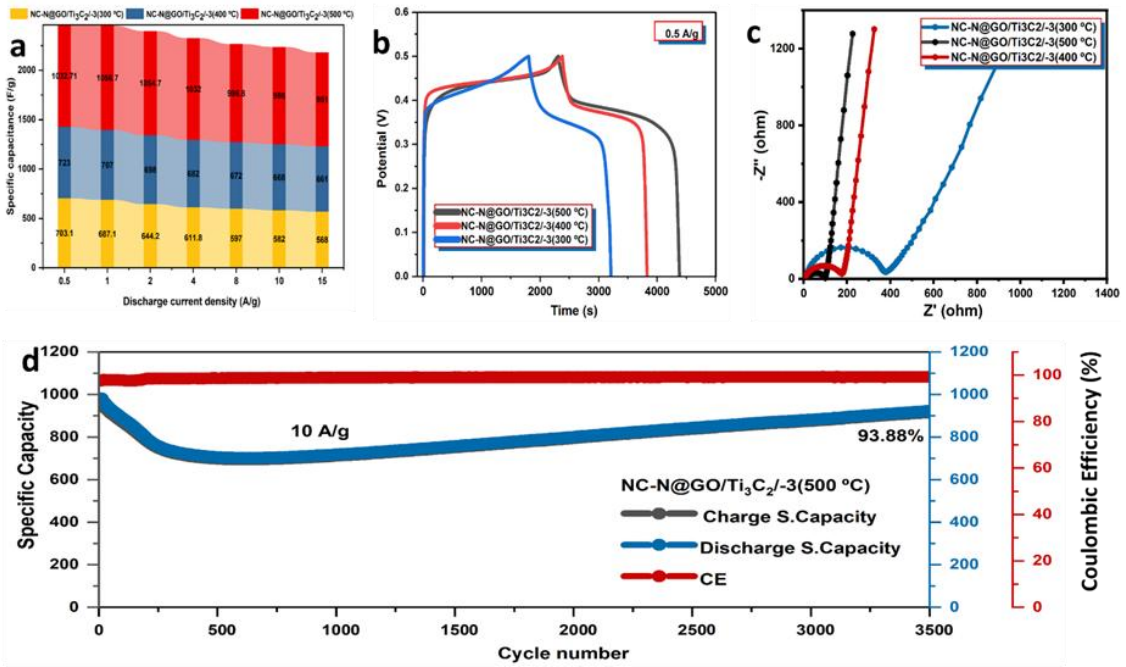

Fig. 5. (a) Histogram of the specific capacitance of the NC-N@GO/Ti_3C_2/-3(500ºC), NC-N@GO/Ti_3C_2/-3(400ºC), and NC-N@GO/Ti_3C_2/-3(300 ºC), electrodes at various current densities. (b) GCD curves of NC-N@GO/Ti_3C_2/-3(500ºC), NC-N@GO/Ti_3C_2/-3(400ºC), and NC-N@GO/Ti_3C_2/-3(300 ºC), electrode at 0.5 A/g. (c) EIS Nyquist plots of NC-N@GO/Ti_3C_2/-3(500ºC), NC-N@GO/Ti_3C_2/-3(400ºC), and NC-N@GO/Ti_3C_2/-3(300 ºC), electrodes and (d) long cycling performance of NC-N@GO/Ti_3C_2/-3(500ºC), electrode at a current density of 10 A/g

Figure 4(g-i) shows the GCD curves of the NC-N@GO/Ti_3C_2/-3(300ºC), NC- N@GO/Ti_3C_2/-3(400ºC) and NC-N@GO/Ti_3C_2/-3 (500ºC) sample electrodes at a constant current density of 0.5 to 15A/g. With a battery-type redox behavior, the NC-N@GO/Ti_3C_2/-3 (500ºC) electrode appeared to have a much longer discharge time (2065s) at a current density of 0.5 A/g than the NC-N@GO/Ti_3C_2/-3 (400ºC) (1446s) and NC-N@GO/Ti_3C_2/-3(300ºC) (1406s). This suggests that the NC-N@GO/Ti_3C_2/-3(500ºC) electrode has improved electrochemical storage stability. Better energy storage performance is indicated by a longer charge/discharge time. and it is primarily attributed to the unique of NC-NGO Features of nanoparticles on the surface of highly conducting reduced GO/Ti_3C_2 sheets, which provide large Enhanced material usage for energy storage activity may result from electrochemical active sites with highly accessible surface area for the transport of electrolyte ions to it. However, the individual discharge schedule NC-N@GO/Ti_3C_2/-3(300ºC) and NC-N@GO/Ti_3C_2/-3(400ºC) electrodes were comparatively short. This is because, at 300 and 400ºC, the NC- LDH@GO/Ti_3C_2/-3 precursor partially structurally changed into a nitride nanoparticle, resulting in a limited surface area for electrochemistry that reduces the exposing active areas in the respective samples to allow electrolyte ion transport. At a current density of 0.5 A/g and based on the discharge duration, the estimated capacitance values were found to be 1032.71 F/g for NC-N@GO/Ti_3C_2/-3 (500ºC), 723 F/g for NC-N@GO/Ti_3C_2/- 3 (400ºC), and 703.1 F/g for NC-N@GO/Ti_3C_2/-3 (300ºC) electrode, respectively. Moreover, Figure 4(G- I) also shows each of the GCD curves of NC-N@GO/Ti3C2/-3 (500ºC), NC- N@GO/Ti_3C_2/-3 (400ºC), and NC- N@GO/Ti_3C_2/-3 (300ºC) electrodes with varying densities of 1, 2, 4, 8, and 10 and15 A/ g. Figure 5a displays the associated calculated specific capacitance values. Because of the lack of redox reactions and resistance at higher current densities, it is evident that the hybrid's capacitance diminishes as the current density rises. But for NC-N@GO/Ti_3C_2/- 3(500ºC), the decline was much less than for NC-N@GO/Ti_3C_2/-3 (400ºC) and NC-N@GO/Ti_3C_2/-3 (300ºC), which had retention rates of 92.2%, 91.4%, and 80.7%, correspondingly, at 15 A/g, In contrast to 0.5 A/g. Although the entire electrode shows excellent rate capability, the NC- N@GO/Ti_3C_2/- 3 (500ºC) shows good electrochemical properties in terms of both capacity and rate capability, indicating the maximum amounts of stored charge Figure 5b. Moreover, Additionally, an investigation using electrochemical impedance spectroscopy (EIS) was conducted to evaluate the resistive characteristics of the NC-N@GO/Ti_3C_2/-3 (500ºC), NC-N@GO/Ti_3C_2/- 3 (400ºC) and NC- N@GO/Ti_3C_2/-3 (300ºC) hybrid electrodes, (Figure 5c). All the Nyquist plots exhibit comparable characteristics: a little, depressed the high-frequency semicircle range represents the resistance to

charge transfer (RCT) and extended no straight line in the area of low frequencies ascribed in relation to the Warburg impedance (Zw), which is connected to the electrolyte diffusion. Based on the Randles equivalent circuit and the complex nonlinear least-squares (CNLS) fitting approach, the charge-transfer resistance (RCT) was determined to be 0.33 Ω for NC- N@GO/Ti_3C_2/-3(500ºC), 0.54 Ω for NC- N@GO/Ti_3C_2/-3(400ºC), and 0.77Ω for NC-N@GO/Ti_3C_2/-3 (300ºC) electrode, which suggests the RCT decreased in the order of NC- N@GO/Ti_3C_2/-3 (300ºC) > NC-N@GO/Ti_3C_2/-3 (400ºC) > NC-N@GO/Ti_3C_2/-3 (500ºC),indicating that NC- N@GO/Ti_3C_2/- 3 (500ºC) holds the lowest RCT, i.e., the quick movement of electrons at the electrode/electrolyte contact. The cycle stability and coulombic efficiency are essential criteria in establishing… The pragmatic uses of SCs that are hybrid [18][19]. To examine the stability of cycling and the coulombic efficiency, NC-N@GO/Ti_3C_2/-3 (500ºC) electrodes were examined at 10 A/g for 3500 GCD cycles as shown in Figure 5d. The NC- N@GO/Ti_3C_2/-3 (500ºC) hybrid electrode's specific capacity was somewhat reduced during the first 250 cycles. This is explained by a first, slow the structure's opening with reduced the activation stage, electrolyte accessibility, followed by a decrease in certain activity as a result of the progressive degradation of the active material within the electrode [20]. Nevertheless, the NC-N@GO/Ti_3C_2/-3 (500ºC) electrode shows capacity fading during the first 250 cycles; their specific capacitance steadily increases throughout the subsequent 3500 cycles. With 100% coulombic efficiency, the NC-N@GO/Ti_3C_2/-3 (500ºC) electrode maintained 93.88% of its initial specific capacitance after 3500 cycles. The NC-N@GO/Ti_3C_2/- 3 (500ºC) hybrid electrode demonstrated noticeably better performance of energy storage and capacity retention compared to the NC-N@GO/Ti_3C_2/-3 (300ºC) and NC-N@GO/Ti_3C_2/-3 (400ºC) hybrid. This might be a result of the stability of the structurthe close interaction connecting NC-N nanoparticles with underlying GO/Ti_3C_2 with NF without requiring due to the highly conductive GO/Ti_3C_2 and the large number of exposed electrochemical active sites of NC-N nanoparticles, a polymeric binder and high-efficiency electron and electrolyte transportation are provided.

4. CONCLUSIONS

This study reports on the synthesis of a bimetallic NiCo-nitride/reduced graphene oxide/Ti_3C_2 MXene hybrid on a flexible nickel foam substrate, denoted as NCN@rGO/Ti_3C_2/NF. This hybrid material was derived from NiCo-layered double hydroxide (LDHs) using a two-step method. Firstly, NC-LDH@rGO/Ti_3C_2/NF nanosheets were grown in situ via hydrothermal growth on the surface of nickel foam. Subsequently, a second step involved thermal annealing in an NH_3 atmosphere (80-100 ml/min) for 3 hours at different temperatures (300, 400, and 500°C) with a 5°C/min heating rate. The electrochemical analysis revealed promising results for the NCN@rGO/Ti_3C_2/NF hybrid electrode annealed at 500°C (denoted as NCN@rGO/Ti_3C_2/NF 500). Specifically, it exhibited remarkable cycle stability, exceptional rate capability of 92.2% at 20 Ag-1, and specific capacitance of 1032.71 Fg-1 at 0.5 Ag-1 and outstanding circle stability of 93.8% after 3500 cycles.

Author contributions: conceptualization: E.E.S., Eris E.S.; data curation: M.K.A.M.A.; investigation: S.S.; methodology: M.I.; project administration: Eris E.S.; resources: M.K.A.M.A.; supervision: Eris E.S. and M.K.A.M.A.; validation: all authors; initial draft writing: E.E.S.; review and editing: Eris E.S.; funding acquisition: Eris E.S. All authors have read and agreed to the published version of the manuscript.

Funding source: Puncak RM Berhad University Community Transformation Center (UPM).

Conflicts of interest: The authors declare that there are no conflicts of interest regarding the publication of this manuscript. We have no financial or personal relationships with individuals or organizations that could influence our work or could be perceived as potential conflicts of interest.

Acknowledgements: The author gratefully acknowledges financial support from Puncak RM Berhad University Community Transformation Center (UPM) and immense contribution of Muhammad Ishaq to the success of this work.

REFERENCES

[1] M.A.A. Mohd Abdah, N.H.N. Azman, S. Kulandaivalu, Y. Sulaiman, (2020), *Review of the use of transition-metal-oxide and conducting polymer-based fibres for high-performance supercapacitors*, Materials & Design, 186, 108199.

[2] E. Elahi, Z. Khalid, Z. Zhang, (2022), *Understanding farmers' intention and willingness to install renewable energy technology: A solution to reduce the environmental emissions of agriculture*, Applied Energy, 309, 118459.

[3] U.K. Pata, A. Samour, (2022), *Do renewable and nuclear energy enhance environmental quality in France?*

A new EKC approach with the load capacity factor, Progress in Nuclear Energy, 149, 104249.
[4] S. Mahmud, M. Rahman, M. Kamruzzaman, M.O. Ali, M.S.A. Emon, H. Khatun, aM.R. Ali, (2022), *Recent advances in lithium-ion battery materials for improved electrochemical performance: A review*, Results in Engineering, 5 , 100472, https://doi.org/10.1016/j.rineng.2022.100472
[5] E. Pargoletti, S. Arnaboldi, G. Cappelletti, M. Longhi, D. Meroni, A. Minguzzi, P. Mussini, S. Rondinini, A. Vertova, (2022), *Smart interfaces in Li-Batteries: near-future key challenges*, Electrochimica Acta, 415, 140258, https://doi.org/10.1016/j.electacta.2022.140258
[6] M.E. Şahin, F. Blaabjerg, A. Sangwongwanich, (2022), *A comprehensive review on supercapacitor applications and developments*, Energies, 15(3), 674, https://doi.org/10.3390/en15030674
[7] D. Lemian, F. Bode, (2022), *Battery-supercapacitor energy storage systems for electrical vehicles: a review*, Energies, 15(15), 5683, https://doi.org/10.3390/en15155683
[8] M.R. Çorapsiz, H. Kahveci, (2022), *A study on Li-ion battery and supercapacitor design for hybrid energy storage systems*, Energy Storage, https://doi.org/10.1002/est2.386
[9] F.A. Permatasari, M.A. Irham, S.Z. Bisri, F. Iskandar, (2021), *Carbon-based quantum dots for supercapacitors: Recent advances and future challenges*, Nanomaterials, 11(1), 91, https://doi.org/10.3390/nano11010091
[10] Y. Yu, C. Li, Y. Fu, W. Yang, (2023), *A group decision-making method to measure national energy architecture performance: A case study of the international energy Agency*, Applied Energy. 330, Part A, 120285, https://doi.org/10.1016/j.apenergy.2022.120285
[11] M.F. Tahir, C. Haoyong, H. Guangze, (2021), *A comprehensive review of 4E analysis of thermal power plants, intermittent renewable energy and integrated energy systems*, Energy Reports, 7, 3517-3534.
[12] H. Budde-Meiwes, J. Drillkens, B. Lunz, J. Muennix, S. Lehner, J. Kowal, D.U. Sauer, (2013), *A review of current automotive battery technology and future prospects*, Proceedings of the Institution of Mechanical Engineers, Part D: Journal of Automobile Engineering, 227, 761-776.
[13] Q. Abbas, M. Mirzaeian, M.R. Hunt, P. Hall, R. Raza, (2020), *Current state and future prospects for electrochemical energy storage and conversion systems*, Energies, 13(21), 5847, https://doi.org/10.3390/en13215847
[14] L. Zhang, X. Hu, Z. Wang, J. Ruan, C. Ma, Z. Song, D.G. Dorrell, M.G. Pecht, (2021), *Hybrid electrochemical energy storage systems: An overview for smart grid and electrified vehicle applications*, Renewable and Sustainable Energy Reviews, 139, 110581, https://doi.org/10.1016/j.rser.2020.110581
[15] S. Ghosh, S. Subudhi, (2022), *Developments in fuel cells and electrochemical batteries using nanoparticles and nanofluids*, Energy Storage, 4, https://doi.org/10.1002/est2.288
[16] Si, W., Yan, C., Chen, Y., Oswald, S., Han, L. Schmidt, O.G., (2013), *On chip, all solid-state and flexible micro- supercapacitors with high performance based on MnO x/Au multilayers*, Energy & Environmental Science, *6*(11), 3218- 3223.
[17] Tahir, M., Pan, L., Idrees, F., Zhang, X., Wang, L., Zou, J.J. Wang, Z.L., (2017). *Electrocatalytic oxygen evolution reaction for energy conversion and storage: A comprehensive review*. Nano Energy, 37, 136-157.
[18] Soualhi, A., Makdessi, M., German, R., Echeverría, F.R., Razik, H., Sari, A., Venet, P. Clerc, G., (2017), *Heath monitoring of capacitors and supercapacitors using the neo-fuzzy neural approach*, IEEE Transactions on Industrial Informatics, 14(1), doi: 10.1109/TII.2017.2701823
[19] Wang, Y., Yin, W., Zeng, J., (2019), *Global convergence of ADMM in nonconvex nonsmooth optimization*, Journal of Scientific Computing, 78, 29- 63.
[20] Uno, M., Tanaka, K., (2011), *Accelerated charge–discharge cycling test and cycle life prediction model for supercapacitors in alternative battery aaplications,* IEEE Transactions on Industrial Electronics, 59(12), 4704-4712.

Received: October 24th, 2024 / Accepted: June 15th, 2025 / Paper available online: June 20th, 2025